ANL/CP--75323

DE93 004244

Simulation of a Particle-Laden Combustion Flow in an MHD Second Stage Combustor

S.L. Chang and S.A. Lottes

Energy Systems Division
Argonne National Laboratory
9700 South Cass Avenue
Argonne, Illinois 60439-4815

Manuscripts submitted to
The 1992 ASME Winter Annual Meeting
Anaheim, California
November 8-13, 1992

Simulation of a Particle-Laden Combustion Flow in an MHD Second Stage Combustor

S.L. Chang and S.A. Lottes
Argonne National Laboratory
9700 South Cass Avenue
Argonne, Illinois 60439-4815

ABSTRACT

An Argonne two-phase combustion flow computer code is used to simulate reacting flows to aid the development of an advanced combustor for magnetohydrodynamic power generation. The combustion code is a general hydrodynamics computer code for two-phase two-dimensional, steady state, turbulent, and reacting flows, based on mass, momentum, and energy conservation laws for multiple gas species. The combustion code includes turbulence, integral combustion, and particle evaporation submodels. The newly developed integral combustion submodel makes calculations more efficient and more stable while still preserving major physical effects of the complex combustion processes. The combustor under investigation is a magnetohydrodynamic second stage combustor in which opposed jets of oxidizer are injected into a confined cross-stream of hot coal gas flow following a first stage swirl combustor. The simulation is intended to enhance the understanding of seed particle evolution in the combustor and evaluate the effects of combustor operation conditions on seed particle evolution and vapor dispersion, which directly affect overall magnetohydrodynamic power generation. Simulation results show that oxidizer jet angle and particle size have great effect on the particle evolution and vapor dispersion. At a jet angle about 130 degrees, particle evaporation rate is the highest because of the highest average gas temperature. For particles having a smaller mean diameter, particle evaporation is more complete and vapor dispersion is more uniform.

NOMENCLATURE

B	Evaporation transfer number
CL	Convergence level
C_d	Particle drag coefficient
Cp	Specific heat (J/mol/K)
D	Combustor hydraulic diameter (m)
H_v	Latern heat (J/kg)
h	Enthalpy (J/kg)
k	Turbulence intensity (J/kg)
K	Gas thermal conductivity (W/mK)
L	Combustor length (m)
L_j	Jet location (m)
$\dot{m}$	Mass flow rate (kg/s)
n	Particle number density (#/m^3)
Nu	Nusselt number
P	Pressure (atm)
r	Particle radius (μm)
Re	Reynolds number
S	Source term of general transport equation (1)
Sc	Schmidt number
T	Temperature (K)
t	time (μs)
U	Gas phase velocity in x-direction (m/s)
V	Gas phase velocity in y-direction (m/s)
x	Axial coordinate (m)

y Vertical cross-stream coordinate (m)
Y_i Mass fraction of a gas species "i"

Greek Letters

ε Turbulence dissipation (J/kg-s)
Γ Diffusion coefficient
μ Viscosity (N-s)
ϕ Stoichiometric mass ratio of oxidizer and fuel
ρ Density (kg/m^3)
τ Richness
θ Gas volume fraction
ξ General flow variable
ζ Extent of reaction

Subscripts

o Reference
b Boiling
fu Fuel species
ir Inert species
pr Product species
ox Oxidizer species
res Residual quantity
s Solid phase variable
sv Seed vapor species
t Turbulence
x Axial direction
y Cross-stream direction

INTRODUCTION

The concept of a magnetohydrodynamic (MHD) power plant, which depends upon the interaction between magnetic fields and an electrically conducting fluid flow to generate electrical power, has attracted much interest in the utility industry because it can attain higher overall efficiency and produce less pollutants compared to a conventional coal-fired power plant [1-2]. For the past ten years, the U.S. Department of Energy has been sponsoring a national program for the development of a proof-of-concept MHD power plant in which industries, universities, and national laboratories have participated. Under this program, Argonne National Laboratory (ANL) provides technical support to the industries who are building the combustor, MHD channel, and other facilities. One major activity at ANL is the use of computer simulation to aid the design of a 50 MWt MHD combustor at TRW [3-6]. The combustor is a two-stage pulverized coal combustor upstream of the MHD generator [7]. The first stage is a swirl combustor operated under a substoichiometric condition to minimize NOx formation while most of slag is removed. A second stage combustor follows the first stage combustor. In the second stage combustor, seed material, i.e., potassium, and additional oxidizer are injected to obtain desired plasma stoichiometry and temperature for successful MHD channel operations.

Among other important issues regarding the operation of a second stage MHD combustor, particle evolution, vapor dispersion, and combustion are studied to determine the effects of combustor operation conditions on MHD channel performance. One of the major concerns is the distortion of gas temperature and seed vapor profiles, caused by poor mixing which may significantly lower the electric conductivity of the gas and subsequently the MHD channel performance. Computer simulation is an efficient and cost-effective tool to help design an advanced combustor because it provides in-depth information about the

two-phase combustion flow and the flexibility to experiment with a wide range of operating conditions at relatively low cost.

Some concerns regarding the simulation of a two-phase combustion flow include computational speed of available computers and stability of a computer code. Recent advances in high-speed supercomputers, computational techniques to solve the coupled partial differential equations of a turbulent flow [8-9], and combustion related modeling, e.g., turbulence, combustion, and jet mixing models [10-11], have encouraged people to develop comprehensive computer models to simulate the complex processes of fluid mixing and reaction in a combustion system. A team of ANL and University of Illinois at Chicago developed a comprehensive combustion flow computer code. The code was originally written for air-breathing propulsion engines [12] and has been modified for various applications in coal-fired combustors [13] and internal combustion engines [14]. For the present study, the code has been modified extensively over the past few years at ANL. The study investigates important issues related to the performance of an MHD second stage combustor. The issues include particle evolution, vapor dispersion, gas ionization, combustion, jet penetration, and fluid mixing. This paper discusses mainly seed particle evolution and vapor dispersion in the combustion flow.

SIMULATION APPROACHES

An ANL two-phase two-dimensional combustion computer code was used to simulate combustion flow patterns in an MHD second stage combustor. The code solves conservation equations for five gaseous species (fuel, oxidizer, product, inert, and seed) and solid particles of various sizes. General conservation laws, expressed by elliptic-type partial differential equations, are used in conjunction with rate equations governing the mass, momentum, enthalpy, species, turbulent kinetic energy, and turbulent dissipation for a two-phase reacting flow. The associated submodels of this code include an integral combustion, a two-parameter turbulence, a particle evaporation, and other interfacial submodels. A newly developed integral combustion submodel replacing an Arrhenius type differential reaction submodel has been implemented to improve numerical convergence and enhance numerical stability. A two-parameter turbulence submodel is modified for both gas and solid phases. The evaporation submodel treats not only particle evaporation but size dispersion. Interfacial submodels use simple correlations to model interfacial momentum and energy transfer.

General Transport Equations

For convenience of numerical formulation the governing transport equations for both gas and solid phases are put in a common form:

$$\frac{\partial J_x}{\partial x} + \frac{\partial J_y}{\partial y} = S_\xi \tag{1}$$

in which ξ is a general flow variable, S is a source (or sink) term, and J's are convective and diffusive flux terms.

Gas species are assumed to be a perfect gas mixture. The convective and diffusive flux terms of a gas flow variable can be written as,

$$J_x = \theta\rho U\xi - \Gamma_\xi \frac{\partial \xi}{\partial x}$$

$$J_y = \theta\rho V\xi - \Gamma_\xi \frac{\partial \xi}{\partial y}$$

$$\text{for } \xi = 1, U, V, Y_{fu}, Y_{ir}, Y_{sv}, \tau, h, k, \text{ or } \varepsilon \tag{2}$$

$$\tau = \frac{\phi Y_{fu} - Y_{ox} + Y_o}{\phi + Y_o} \tag{3}$$

$$Y_{pr} = 1 - Y_{fu} - Y_{ox} - Y_{ir} - Y_{sv} \tag{4}$$

where, θ is gas volume fraction, ρ is density, Γ is effective diffusion coefficient, ϕ is the stoichiometric mass ratio of oxidizer and fuel, and Y_o is a reference concentration. U and V are velocity components, Y_f, Y_{ir}, Y_{sv} are mass fractions of gaseous species of fuel, inert, and seed vapor, respectively, τ is richness, h is enthalpy, k is turbulent kinetic energy, and ε is turbulent dissipation rate. Note that concentrations of oxidizer and product species are not solved directly from a transport equation. Since a transport equation with no source term is more stable in a solution routine, the transport equation for oxidizer concentration is replaced by a richness equation which eliminates the reaction sink term if richness is defined as equation (3). As soon as the richness and fuel species transport equations are solved, oxidizer concentration can be easily obtained from equation (3). After all the other species are solved, product concentration can be obtained from the species conservation equation (4).

The solid phase equations include number density (n), velocities (U_s, V_s), and temperature (T_s) equations. For each particle size group, the convective and diffusive flux terms of number density are:

$$J_x = nU_s - \Gamma_\xi \frac{\partial \xi}{\partial x}$$

$$\text{for } \xi = n \tag{5}$$

$$J_y = nV_s - \Gamma_\xi \frac{\partial \xi}{\partial y} \text{ in 0}$$

and the flux terms of velocities and temperature are:

$$J_x = nU_s\xi$$

$$\text{for } \xi = U_s, V_s, \text{ or } T_s \tag{6}$$

$$J_y = nV_s\xi$$

The source term of particle number density accounts for particle evaporation, while the diffusion term accounts for particle dispersion due to interaction with the turbulence of the gas phase. The interactions between phases are all included in the source terms. For example, a momentum sink in gas flow accounting for particle drag effects is also a momentum source for the solid flow.

Associated Submodels and Empirical Correlations

To determine source terms and effective diffusion coefficients of the transport equations for both gas and solid phase flow variables, submodels and empirical correlations are needed. For the source terms of the transport equations of fuel concentration and enthalpy, a submodel is required to determine fuel consumption and heat release rates. For seed vapor concentration and particle number density, a submodel is required to determine particle evaporation and size dispersion rates. For gas and solid velocities, correlations of interfacial drag force are required to determine momentum exchanged between phases. For gas enthalpy and solid temperature, correlations of interfacial heat transfer are required to determine energy exchange between phases. For the effective diffusion coefficients of all transport equations, a submodel is required to determine turbulent diffusivity for both gas and solid phases.

An integral one-step combustion submodel has been developed to make numerical calculation of the complex combustion processes in the present study faster and more efficient while still preserving the major physical effects of the combustion on the flow development. The model replaces a previous

differential combustion model which used an Arrhenius type rate equation. The new model is found to substantially enhance the numerical stability of reacting flow computations with the computer code. The model assumes that the overall reaction progress and its physical effects can be expressed by empirical correlations or tabulated data relating the extent of reaction (or the fraction of fuel consumed) and the accumulated heat of combustion to a flow time scale instead of a reaction time scale. Detailed kinetics calculations provide data to tabulate or correlate an extent of reaction as a function of time. For this study, detailed kinetics calculations are carried out using NASA's General Chemical Kinetics Program [15]. Computed temperature and extent of reaction is plotted against time in Figure 1. Note that the reaction pressure is 5.7 atm and reference temperature T_o is 2950 K. For the combustion processes, a correlation of the extent of reaction ζ is written as,

$$\begin{aligned} \zeta &= 0.1495 \ln(80t + 1), && \text{for } t \le 0.1 \ \mu s \\ \zeta &= 1 - \exp(-0.705t^{0.25}) && \text{for } 0.1 < t \le 0.25 \ \mu s \\ \zeta &= 0.57 - 0.1774 \exp(-0.78(t-0.25)^{1.04}) && \text{for } t > 0.25 \ \mu s \end{aligned} \tag{7}$$

A similar correlation for heat of combustion is also obtained from the plotted results. These correlations are incorporated into the source terms of the gas enthalpy and fuel concentration transport equations. More details of the integral combustion submodel are reported in reference 4.

A two parameter turbulence submodel is used to simulate the turbulent transport of gas and solid phases. Based on the work of Launder and Spalding [8], turbulent viscosity μ_t is defined as:

$$\mu_t = 0.09 \rho \frac{k^2}{\varepsilon} \tag{8}$$

in which the two turbulent parameters k and ε are solved by two turbulent transport equations. For gas momentum equations, effective viscosity (or diffusion coefficient) is defined as the sum of gas viscosity and turbulent viscosity. For equations of other gas flow variables, effective diffusivities are assumed to be proportional to the effective viscosity. Similarly, diffusion coefficients for particle number density are assumed to be related to gas turbulent viscosity and account for the effect of particle size dispersion. The larger the particle, the smaller the diffusivity. The empirical formula for the particle diffusion coefficient used in this computer code is based on the work of Ward et al. [16].

$$\Gamma_n = \frac{\mu_t}{0.9 \rho (1 + 2r + 0.06r^2)} \tag{9}$$

where r is particle radius (in μm).

Treating a spray of particles in the Eulerian framework, the number density is taken to be a function not only of the coordinates x and y but also of the particle radius. Zhou and Chiu [10] used a simple mathematical function used to represent the inlet size distribution of a spray. A similar size dispersion formula is used for represent the inlet seed particle flow. The formula is:

$$\frac{dn}{dr} = a r^4 \exp(-br^4) \tag{10}$$

where a and b are constants to be determined from total particle number density and mean particle radius.

A transport equation for number density of a particle size group is derived by doing a balance over a (x,y,r) space. Similar to the discretization of the x and y coordinate to yield the physical space computational grid, the particle size coordinate, r, is discretized to yield a set of particle size groups. The

number density transport equation accounts for not only the fluxes in the physical coordinates but the rate of shift of the particle size spectrum due to particle evaporation, which causes evaporating particles to move from larger to smaller size groups. When particles evaporate, particle size decreases, vapor is added to the seed vapor, momentum is added to the gas momentum, and latent heat is subtracted from the gas enthalpy. A correlation is used to predict particle evaporation rate in a convective field.

$$\dot{m} = 4 \pi r \, (K/Cp) \, Nu_e \ln(1+B) \tag{11}$$

where

$$Nu_e = 1 + .276 \, Re^{.5} \, Sc^{.33} \tag{11a}$$

and

$$B = \frac{Cp \, (T - T_{b)}}{H_v} \tag{11b}$$

In the above equations, K is gas thermal conductivity, Cp is gas specific heat, and Nu, Re, Sc, and B are Nusselt, Reynolds, Schmidt and evaporation transfer numbers. Reynolds number is defined using slip velocity.

Gas thermal conductivity increases with temperature and decreases with pressure. In the temperature range of this study from 300 to 3000 K, gas thermal conductivity varies more than an order of magnitude and pressure dependency becomes apparent at high temperature (above 2000 K). In a two phase flow variation of thermal conductivity of the gas with temperature has a large effect on the rate of heat exchange between the phases. By using the published data, an empirical correlation of gas thermal conductivity has been established including both temperature and pressure (P) dependency. The correlation is written as,

$$\begin{aligned} K &= 0.0223 + 0.0977 \, (T - 250)/1550, && \text{for } T < 1800 \text{ K} \\ K &= 1 + 0.0977 \, (T - 1800)/1550 + \\ &\quad (0.2904 - 0.182 \, (P\text{-}1)/9) \, ((T - 1800)/1200)^{2.93} && \text{for } T > 1800 \text{ K} \end{aligned} \tag{12}$$

In a two-phase flow, the solid flow is driven by the gas flow via the shear force generated between phases which depends on the velocity differential between phases. The larger the velocity differential, the bigger the interfacial force. The empirical formula for the particle drag coefficient used in the combustion code is,

$$C_d = (24/Re) \, (1 + .15 \, Re^{.687})/(1+B) \tag{13}$$

Similarly, the empirical formula for particle heat transfer coefficient is written in a Nusselt correlation,

$$Nu = 2 + .654 \, Re^{.5} \, Sc^{.33} \tag{14}$$

The momentum transfer rate between phases needed for the source terms of gas and particle momentum transport equations is calculated based on the drag coefficient and a slip velocity. The convective heat transfer rate between phases needed for the source terms of gas enthalpy and particle temperature transport equations is calculated based on the Nusselt coefficient and a slip temperature (temperature difference between gas and solid phases).

Numerical Approaches

Figure 2 shows the combustor under the investigation, an idealized rectangular box consisting of four solid side walls (front, back, top and bottom), an inlet for gas and particle flow (left), oxidizer injection slots on both top and bottom walls representing distributed injection holes for the two-

dimensional computation, and the exit (right). A two-dimensional computational domain is defined in a cross-sectional area in the middle of the combustor away from the viscous effects near the front and back walls as shown in Figure 2. The two-dimensional grid point system uses a horizontal x-axis and a vertical y-axis, and has the origin at the lower left corner. Evenly spaced grid points are used for the y-axis and variably spaced grid points are defined for the x-axis depending on the jet location. Dense grid points are selected near the jet opening where large flow property gradients are expected.

A convergence and grid sensitivity study was conducted to identify convergence levels for both gas and particle phases in which computed variables have converged to four or more decimal digits over nearly all of the grid points, to identify a level of grid refinement in which computed variables change little upon further grid refinement, and to identify a number of particle size groups (the discretization parameter for the particle phase) in which computed particle variables change little upon further refinement of particle size space. This study was important, first to gain confidence in the computed results, verifying that they will not change significantly, if more grid points or particle size intervals are added of if the convergence level is driven down further. Second, cost including computer CPU time and memory space of a two-phase combustion calculation increases by a factor proportional to the number of particle size groups. Computing time for a case with five particle size groups takes more than three times that of a gas phase case. Determining the minimum amount of computational resources necessary to obtain good quality computational results with a relatively high confidence is a necessary step to control costs and allow a thorough parametric study to be done for a two-phase combustion flow simulation.

For convenience of discussion and comparison, a convergence level CL is defined as:

$$CL = -\log \frac{\dot{m}_{res}}{\dot{m}_o} \tag{15}$$

where $\dot{m}_o$ is the reference (or inlet) mass flow rate, and $\dot{m}_{res}$ is either the maximum or average mass residual from the gas phase continuity equation computed over all of the computational cells. The larger the CL number the better the calculation converges.

Comparisons of centerline or exit temperatures for various levels of convergence or grid refinement were made. Temperature was the variable chosen to illustrate the results because temperature in a combustion computation is somewhat more sensitive than other variables to convergence level and grid refinement. Figure 3 shows dependence of centerline temperature on the level of convergence in terms of maximum mass residual on an optimum sized grid. Results indicate that a convergence level of 9 or above for the maximum mass residual is adequate for a gas-phase combustion calculation to converge to four or more decimal digits over all of the grid points for all major variables.

The effect of y-grid refinement on the computed results was investigated. Computed results at a convergence level of 9 for cases with different numbers of y-nodes were compared. For cases with more than 32 nodes, computed results are found to be nearly the same. An even number was chosen because for symmetric two phase cases, this choice yields a symmetry line at grid center rather than a cell at grid center, and two phase computations were found to be much more stable for the symmetry condition with this choice of grid layout. A similar series of grid refinements was done for the x-grid and a grid with 54 x-nodes was chosen. A gas phase combustion calculation for a 54 by 32 grid requires about six minutes of CPU time on a CRAY/XMP supercomputer.

Next, the effect of size group refinement on particle convergence level was studied. A particle convergence level is defined based on particle mass conservation with the same formula, eq.(15).

High levels of convergence for the particle phase have been found more difficult to achieve than that of the gas phase. Particle stagnation cells, computational cells were the particle flow stagnates or nearly stagnates due to opposed gas flow, are often numerically unstable and require special treatment. In

the gas phase, gas flow stagnation points do not have a similar problem because the pressure term always acts to turn the flow around stagnation points. In the particle phase, there is no term in particle phase transport equations which plays a role corresponding to that of the pressure term in the gas phase equations. Fortunately, the particular way in which particle stagnation cells are handled does not appear to significantly affect converged values of particle variables over the rest of the grid away from the particle stagnation cells. Results indicate that a convergence level of 5 or above for the maximum particle mass residual is adequate for a solid-phase calculation.

Particle number density results for various particle convergence levels were compared. A particle phase convergence level of 5 appeared to be adequate for the particle phase. Furthermore, a comparison of the effect of varying the number of particle size groups on the gas phase seed concentration was made. In the present study of modeling the two-phase combustion flow, particle evolution and seed vapor dispersion are of primary interest. Results of centerline seed vapor concentration for a vaporizing particle flow using a number of particle size groups ranging from 3 to 6 are shown in Figure 4. Based on these results five particle size groups appears to be the minimal requirement to model the particle phase processes.

Based on the sensitivity study, a grid of 54 by 32 nodes representing the combustor configuration shown in Figure 2 and five particle size groups representing the size distribution are selected for two-phase combustion flow calculations. Computed results are used when a gas phase convergence level of nine and a particle phase convergence level of five are achieved.

Most flow variables are assigned values at the inlet plane and jet openings in the side walls. A reference pressure is assigned at the midpoint of the inlet plane. Patankar's locally one way flow assumption [9] is applied to the outflow boundary, eliminating the need to specify the values of flow variables at the outflow boundary. In this formulation, the streamwise diffusion coefficients are taken to be zero at the outflow boundary. The side walls are impermeable for gas. Solids are allowed to deposit on the walls. A momentum wall function is used to bridge the near wall boundary layer. A staggered grid system was used for the numerical calculation, with the gas velocity components stored on the cell surfaces and all other physical quantities stored at the nodal points of each cell (or scalar cell). The governing partial differential equations are transformed into algebraic equations by integrating over the computational cell. These algebraic equations are solved using a line-by-line sweep in the primary flow direction to avoid numerical asymmetry.

A procedure added to the computer code dynamically alters the computational grid to adjust the area of the jet and maintain a specified jet mass flow rate constant during iteration toward the solution. The width of the jet slots is adjustable during computation so the total jet mass flow rate and jet velocity are fixed as defined by input values. When the jet velocity is specified at the jet inlet, the compressibility of jet inlet conditions affects the mass conservation of jet flow because pressure is no longer a free boundary condition, but rather needs to be determined from the flow solution in the interior.

RESULTS AND DISCUSSIONS

A parametric study has been performed to study combustion flow patterns and particle-flame interactions, and to investigate the effect of particle size and inlet profiles on seed vapor dispersion. The common flow conditions used for the following calculations are summarized in Table I.

Combustion Flow and Particle Evolution Patterns

A baseline case of two-phase combustion flow has been computed. The baseline case assumes a uniform inlet particle number density and an average inlet particle size (or diameter) of 34 μm. Baseline two-phase combustion flow patterns are shown in Figures 5-7. Figures 5a and 5b show gas and particle velocity vectors; Figures 6a and 6b show gas and particle temperature contours; Figure 7a shows total particle number density contours; and Figure 7b shows seed vapor concentration contours. In Figure 5,

vector length represents velocity magnitude; inlet gas velocity is 29.6 m/s; and inlet particle velocity is 25 m/s. In Figure 6, temperature is normalized by the reference temperature 2950 K; inlet gas temperature is 1974 K; particle inlet temperature is 300 K; and jet temperature is also 300 K. In Figure 7a, total number density summing number density of five size groups is normalized by its inlet value 528×10^6 #/m^3. In Figure 7b, seed vapor concentration is expressed by mass percentage; inlet seed vapor concentration is zero; and inlet seed particle mass flow rate is about 1% of exit gas mass flow rate.

With 130 degree counter-flow injection, intense mixing occurs upstream of the injectors, and the flame is established in this intense mixing zone (Figure 4a). Because the jets penetrate deeply into the main flow, large vortices form behind the jets (Figure 5a), and the flame follows the vortex boundary from the upstream, where fuel and oxidizer first meet, around toward chamber center as the oxidizer jets are turned downstream. The flame then continues to develop as a diffusion flame in the mixing layer between fuel and oxidizer in the downstream. Computed results show that the fluid temperature, the fuel concentration, and the oxidizer concentration at the exit are approaching their respective equilibrium values.

In Figure 5, particle and gas show different flow patterns because of slip velocities. Slip velocity between gas and particles diminishes as particles move downstream in the combustor. The smaller the particle the smaller the slip velocity. For particles smaller than 5 μm, slip velocity is negligible. In Figure 6, particle temperature lags gas temperature as particles are heated up by the gas. Slip temperature (or temperature difference) between gas and particles becomes smaller as particles move downstream the combustor until the particle temperature reaches boiling temperature. The smaller the particle the faster the particle temperature reaches boiling temperature. For particles smaller than 5 μm, particle temperature reaches boiling temperature almost imediately. Figure 7a shows that some particles are pushed by the oxidizer jets to the combustor center before they are vaporized; some particles are trapped by the wall near the oxidizer jet openings; and some particles escape the combustor. At boiling temperature, T_b = 1595 K, particles vaporize at a rate depending on the surrounding gas temperature and slip velocity. Figure 7b shows that seed vapor is formed primarily near the combustor center and is gradually diffused to the side walls as the gas flows downstream.

The predicted combustion flow patterns for various oxidizer jet angles have been computed and compared. Oxidizer jet angle is found to have great effect on combustion performance as well as particle evolution. Predicted flow patterns of a 50 degree oxidizer jet injection case contrast sharply with those of 130 degree oxidizer jet injection described above. For 50 degree injection the oxidizer jets do not penetrate significantly into the main flow, but rather are rapidly turned into the downstream forming a thick high gradient region near the walls. This flow configuration creates a nearly pure diffusion flame with a relatively low rate of mixing and combustion compared to the 130 degree injection case. Clearly, the change of combustion flow patterns affects the combustion performance, especially, the uniformity of temperature profile at the exit plane (or exit thermal mixedness), which has great influence on the particle vaporization and vapor dispersion. The dependence of exit seed vapor mixedness on jet angle for a two-phase combustion flow is found similar to those of thermal mixedness for gas combustion flow and fluid mixedness for non-reacting flow. A large increase in particle vaporization occurs when going from co-flow injection to counter-flow injection. The angle range for most effective particle vaporization and vapor dispersion is approximately 130 degrees.

Although there is no experimental data for direct comparison with the two-phase combustion calculations, the prediction of optimum jet angle appears to be in general agreement with preliminary testing results and the predicted optimum jet angle matches the design of TRW's MHD second stage combustor [7].

Effect of Particle Size on Seed Vapor Dispersion

From the baseline results, particle size is found to have significant effects on particle evolution.

Computations were performed for four different inlet mean particle diameters in the range 8.5 to 68 μ m. One set of computations assumed a uniform distribution of particles across the chamber inlet. A second set of computations assumed a normal distribution with the peak of the inlet particle number density occurring at the chamber midplane.

Results presented in the next few paragraphs are for cases of uniform inlet number density distribution. The evolution of total number density (the sum of number density over the particle size spectrum at a point) along a line of grid points adjacent to the chamber center line and here after referred to as chamber center evolution is shown in Figure 8 for various inlet mean particle diameters. The injected particles are assumed to be cold relative to the incoming gas stream from the first stage combustor. Before vaporizing, the particles must be heated by the surrounding gas. This prevaporization heating takes longer for large particles than for small particles, and therefore number densities for cases with larger size particles remain higher into the downstream of the chamber. A second process affecting particle number density at chamber center is the screening effect of the jets. The main flow is forced toward chamber center in order to pass the sidewall oxidizer jets, and particles are pushed into the chamber center in this process through drag effects. For the smallest particle case (mean diameter 8.5 μ m) most of the vaporization takes place upstream of the jets at (X/D = 0.66), and therefore, the total centerline number density for this case drops rapidly and continuously due to vaporization as the particle flow moves downstream from the inlet. For the 34 μ m diameter case, a large buildup of particle number density in chamber center is seen in Figure 8 due to the screening effect of the jets. Larger particles take significantly longer time to heat and to vaporize than smaller particles. As shown in Figure 8 for the 34 μ m diameter case, center line number density remains above 40 percent of the inlet value all the way to the exit plane. Results show that for the larger inlet mean particle diameter cases (34 μ m and above), significant numbers of particles escape the chamber before vaporization has been completed near the chamber center.

Of course, number density is not a measure of the mass fraction of seed particles that has vaporized at the chamber exit plane, because as particles vaporize they decrease in size, but they still exist and contribute to the total number density until they have vaporized completely and their diameter becomes practically zero. The fraction of injected particle mass vaporized for the 34 μ m case is about 90 percent, for the cases of smaller particles (17 and 8.5 μ m mean inlet diameter) over 98 percent was vaporized by chamber exit, while for the largest mean inlet diameter case tested (68 μ m), the fraction of inlet particle mass vaporized dropped to about 40 percent.

Both the extent of vaporization and the location of vaporization vary with mean inlet particle size over the range of particle sizes tested. As previously noted, particles that have not vaporized upstream of the jets are pushed via interfacial drag to the chamber center. Due to the presence of recirculation zones behind the jets, the spreading of the main flow back across the chamber in the downstream of the jet location is gradual. As a consequence, the component of particle drag away from the center line in the downstream of the jets is very small, and particles tend to remain concentrated near the chamber center line in the region downstream of the jets. Therefore when vaporization of larger particles occurs downstream of the jets due to longer prevaporization heating delay and longer vaporization time, seed vapor is primarily deposited near the chamber center in that downstream region. In the MHD application, a uniform distribution of seed vapor is desirable, and delayed vaporization for larger seed particle sizes makes the exit distribution of seed vapor much less uniform. This result is shown is Figure 9 where exit seed vapor concentration profiles are plotted. For the cases with mean inlet particle diameter of 8.5 and 17 μ m, seed vapor distribution at the exit is fairly uniform. For the 8.5 μ m case much of the vaporization occurs upstream of the jets. In the 17 μ m case a large portion of the vaporization occurs downstream of the jet inlet plane, and therefore near the chamber center, however, most of the vaporization still occurs far enough upstream of the chamber exit for the vapor deposited near chamber center to spread out across the chamber via diffusion and turbulent transport, giving a relatively uniform seed vapor distribution at the chamber exit plane. For the case of 34 μ m mean inlet diameter particles, much of the vaporization occurs too far into the downstream of the chamber for the spreading effects of diffusion and turbulence to have much impact by the time the flow reaches the chamber exit, and

therefore the seed vapor distribution for the 34 μ m inlet mean particle size case has a pronounced peak in the chamber center (Y/D = 0.5), Figure 9.

When the evolution of seed vapor concentration along the center line is compared for various mean inlet particle sizes, it is found that the onset of vaporization is delayed as mean inlet particle size increases. The maximum value also increases with mean inlet particle size, showing that a greater portion of vaporization takes place near chamber center for larger sized particles, a consequence of particle flow dynamics explained in previous paragraphs.

The presence of vaporizing particles in the flow may affect the combustion progress through heat removed from the gas phase for vaporization, dilution of reactants with seed vapor, slight changes in hydrodynamics due to momentum transfer via interfacial drag, and turbulent kinetic energy removed from the gas phase also due to interfacial drag. In the cases tested, which all used a particle loading of approximately 1 percent by mass, the effect of inlet mean particle size on combustion progress, measured by the evolution of center line fuel concentration, was small. The peak gas temperature drops about 50 K due to the presence of particles.

A second set of cases was computed with a normal distribution of inlet number density. This distribution concentrates particles in the chamber center at the inlet and simulates an injector source of particles in the near upstream of the inlet plane. As noted in the discussion of cases with a uniform particle distribution at the inlet, the screening effect of the oxidizer jets at X/D = 0.66 tends to push the particle flow into the chamber center. The difference between a uniform inlet distribution of particles and a normal distribution with number density peak in the center is primarily a consequence of processes upstream of the jets. The main difference in vaporization and seed vapor distribution occurring between the uniform and normal distribution of particles at the inlet is an increase in the portion of vaporization occurring near the center line primarily for the cases of smaller inlet mean particle size. Because this increase in near center deposition of seed vapor occurs primarily upstream of the jets, sufficient length of chamber remains for much of this vapor to spread out over the chamber cross section as the flow proceeds downstream. Consequently, seed vapor distributions are slightly but not dramatically less uniform at the chamber exit for the normal inlet distribution cases than for the uniform inlet distribution cases, and the effect is more pronounced for the smaller inlet mean particle sizes.

The computation of each case also uses a normal distribution of particle sizes about the inlet mean particle size to represent the inlet particle size spectrum. For purposes of discrete computation on a digital computer, the size spectrum is divided into a number of particle size bands or groups. The evolution of particle number density along the center line for the case with an inlet mean particle diameter of 34 μ m is shown in Figure 10 for individual size groups. The vaporization process in a particular size band decreases the number density in that size group and increases the number density in the next smaller size group. The screening effect of the jets also tends to increase number density in all size groups as particles are pushed to the center.

CONCLUSIONS

A comprehensive computer code has been developed for the simulation of a particle laden combustion flow in an MHD second stage combustor. The simulation is used to investigate the effects of combustor operation parameters on seed particle evolution and vapor dispersion because the cross-sectional uniformity of gas temperature and seed vapor concentration is crucially important to the performance of the overall MHD power generation. A sensitivity study suggests a grid of 54 by 32 nodes to represent the combustor configuration and five particle size groups to represent the size distribution for a two-phase combustion flow simulation. Computed results are used when a gas phase convergence level of nine and a particle phase convergence level of five are achieved. Particle flow patterns are found different than gas flow patterns because of slip velocities. Slip velocity and slip temperature of smaller particles become negligible. In the combustor, many particles are pushed by the oxidizer jets to the combustor center for vaporization and some particles may deposit on the walls. Depending on the particle

size, some particles may escape the combustor before they are completely vaporized. Most particles are heated up to boiling temperature and vaporize in combustor center, then, seed vapor diffuses to the side walls. Results also show that oxidizer jet angle and particle size have great effect on the particle evolution and vapor dispersion. At a jet angle about 130 degrees, particle evaporation rate is the highest because of the highest average gas temperature and combustion efficiency. For seed particles having a smaller mean diameter, particle vaporization in the combustion flow is more complete and vapor dispersion at the exit is more uniform.

ACKNOWLEDGEMENT

This work was supported by U.S. Department of Energy, Assistant Secretary for Fossil Energy, Under Contract W-31-109-ENG-38. Information and suggestion provided by TRW, Inc. are greatly appreciated.

REFERENCES

1. Chang, S.L., G.F. Berry, and N. Hu, "System Analysis of High Performance MHD Systems," Proc. of 23rd Intersociety Energy Conversion Engineering Conference, Vol. 4, pp. 455-459 (1988).

2. Carter C. and J.B. Heywood, "Optimization Studies on Open-Cycle MHD Generators," AIAA Journal, Vol. 6, pp. 1703-1711 (1968).

3. Chang, S.L., S.A. Lottes, and G.F. Berry, "Computation of Two-Dimensional Non-Reacting Jet/Main Flow Mixing in an MHD Second Stage Combustor," Numerical Heat Transfer, Part A, 20(2):1-14 (1991).

4. Lottes. S.A., and S.L. Chang, "Simulation of Combustion Processes in an MHD Second Stage Combustor," Proc. of 29th Symposium of Engineering Aspects of Magnetohydrodynamics, New Orleans, LA, pp.III.4.1-11 (1991)

5. Berry, G.F., S.L. Chang, S.A. Lottes, and W.A. Rimkus, "Multi-Dimensional Computer Simulation of MHD Combustor Hydrodynamics," AIAA 22nd Fluid Dynamics, Plasma Dynamics & Lasers Conference, Honolulu, Hawaii, AIAA 91-1511 (June 24-26, 1991)

6. Lottes, S.A., S.L. Chang, and G.F. Berry, "Effects of Jet Ports Arrangement on Three-Dimensional Non-Reacting Jet-Gas Mixing in an MHD Second Stage Combustor," Proc. of 25th Intersociety Energy Conversion Engineering Conference, Reno, Nevada, 2:468-473 (August 12-18, 1990).

7. Grove, A., "Design Study of MHD Coal-Fired Combustor Second Stage," 29th Symposium on Engineering Aspects of Magnetohydrodynamics, New Orleans, LA, pp.III.3.1-III.3.9 (June 18-20, 1991).

8. Launder, B.E., and D.B. Spalding, "The Numerical Computation of Turbulent Flows," Computer Methods in Applied Mechanics and Engineering, Vol. 3, pp. 269-289 (1974).

9. Patankar, S.V., "Numerical Heat Transfer and Fluid Flow," McGraw-Hill Book Company (1980).

10. Zhou, X.Q., and H. Chiu, "Spray Group Combustion Processes in Air Breathing Propulsion Combustors," Paper AIAA-83-1323, AIAA/SAE/ASME 19th Joint Propulsion Conference, Seattle, Washington (1983).

11. Patankar, S.V., D.K. Basu, and S.A. Alpay, "Prediction of the Three-Dimensional Velocity Field of a Deflected Turbulent Jet," Journal of Fluids Engineering, 99:758-762 (1977).

12. Jiang, T.L., and H.H. Chiu, "Advanced Modeling of Spray Combustion Process in Air Breathing Propulsion Combustors," AIAA-87-0067, AIAA 25th Aerospace Science Meeting, Reno, Nevada (1987).

13. Lottes. S.A., and S.L. Chang "Interactions of Turbulent Eddies and Combustion in an MHD Second Stage Combustor," Proceedings of the 26th Intersociety Energy Conversion Engineering Conference, Boston, MA, 3:69-74 (August 4-9, 1991).

14. Chang, S.L., and C.S. Wang, "Thermal Radiation and Spray Group Combustion in Diesel Engines," ASME Winter Annual Meeting, Boston, Mass., HTD-81:25-34 (December 13 , 1987).

15. Bittker, D.A. and V.J. Scullin, "General Chemical Kinetics Computer Program for Static and Flow Reactions, with Application to Combustion and Shock-tube Kinetics," NASA TN D-6586 (1972).

16. Ward, P., N. Collings, and N. Hey, "A Comparison of Simple Models of Turbulent Droplet Diffusion Suitable for Use in Computations of Spray Flames," ASME 82-WA/HT-2 (1982).

APPENDIX:

Table I Common Flow Conditions

Combustor Aspect Ratio (L/D) =	3.84
Pressure (atm) =	5.7
Inlet Gas Temperature (K) =	1974
Particle Boiling Temperature (K) =	1594
Inlet Gas Velocity (m/s) =	29.3
Inlet Particle Velocity (m/s) =	25
Bulk Seed Mass Fraction (%) =	1
Overall Stoichiometric Ratio =	1.0
Inlet Fuel Concentration =	0.368
Inlet Inert Concentration =	0.390
Inlet Product Concentration =	0.242
Jet Mass Flow Rate (kg/s) =	0.454
Jet Temperature (K) =	300
Jet Location (L_j/ D) =	0.66
Jet Angle (deg.) =	130
Jet Oxidizer Concentration =	1.0

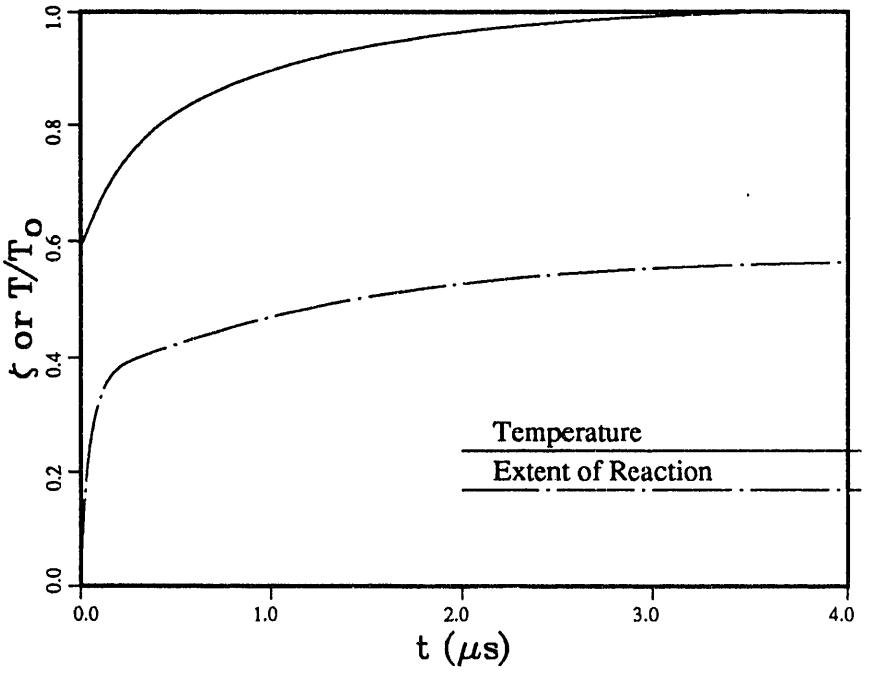

Figure 1 Progress of coal-gas combustion with full kinetic reactions

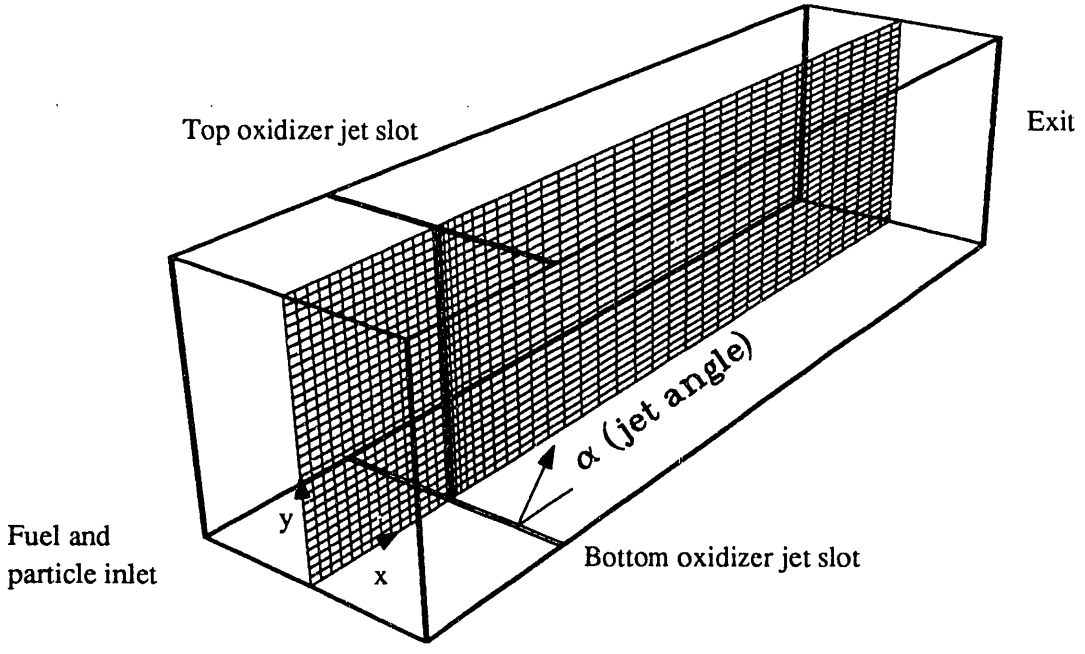

Figure 2 Combustor geometry and a two-dimensional computational grid with 54 by 32 nodes

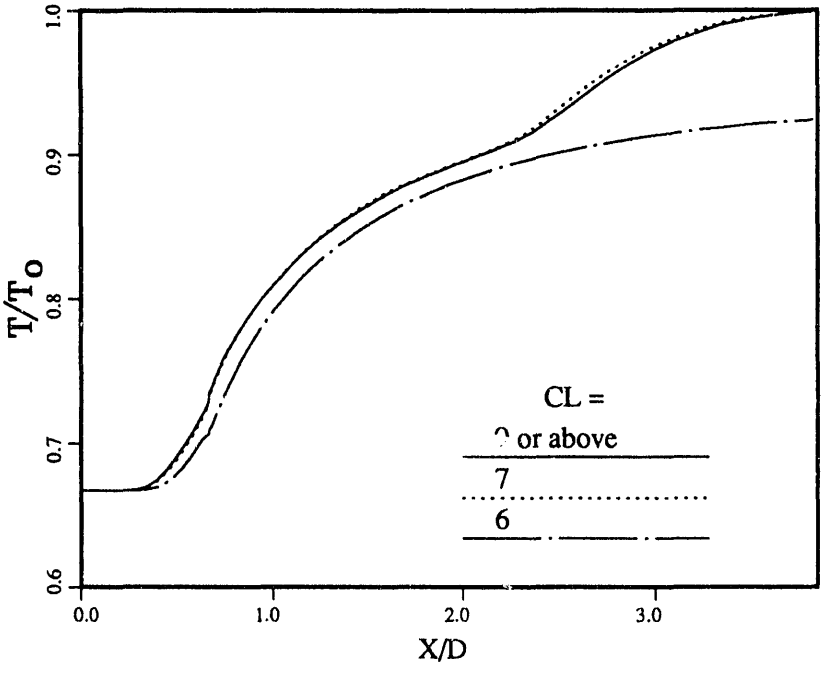

Figure 3 Development of centerline gas temperature for various convergence levels

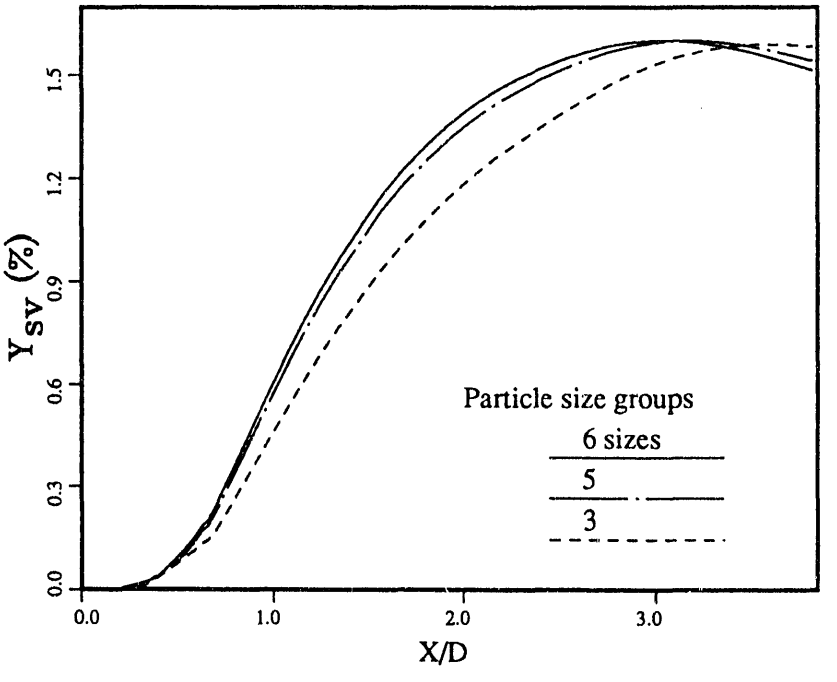

Figure 4 Development of centerline seed vapor concentration for various numbers of particle size groups

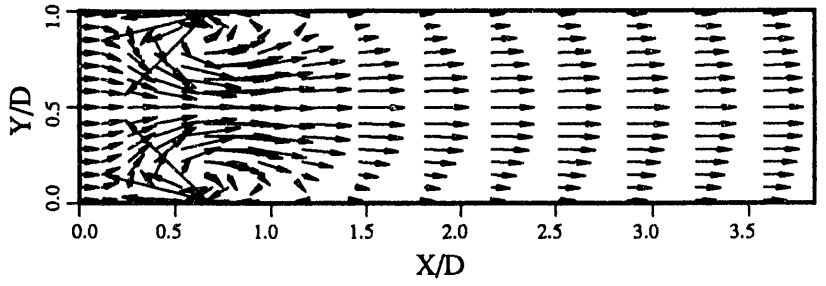

(a) Gas

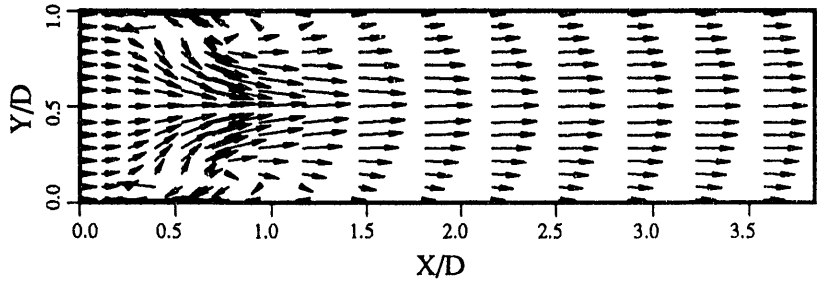

(b) Particles (30 microns)

Figure 5 Comparison of gas and particle flow patterns

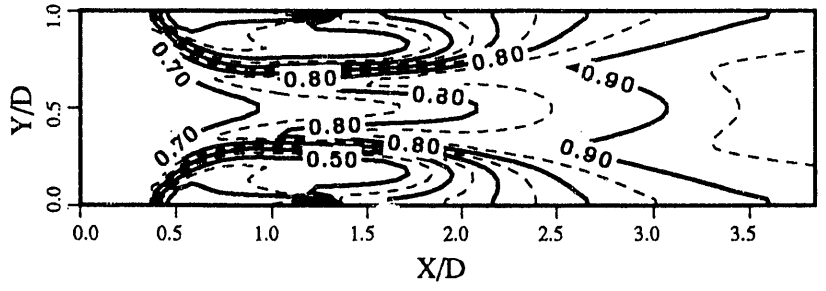

(a) Gas

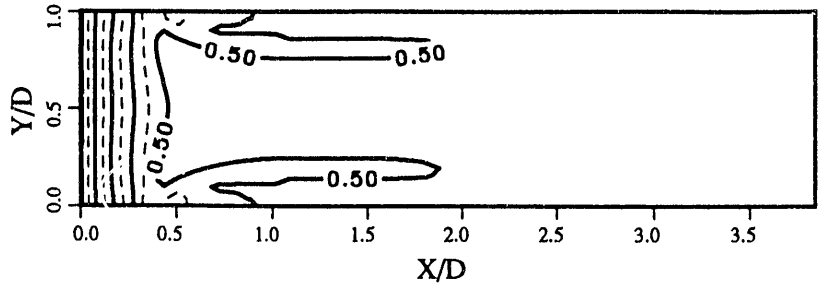

(b) Particles (30 microns)

Figure 6 Comparison of gas and particle temperature distributions

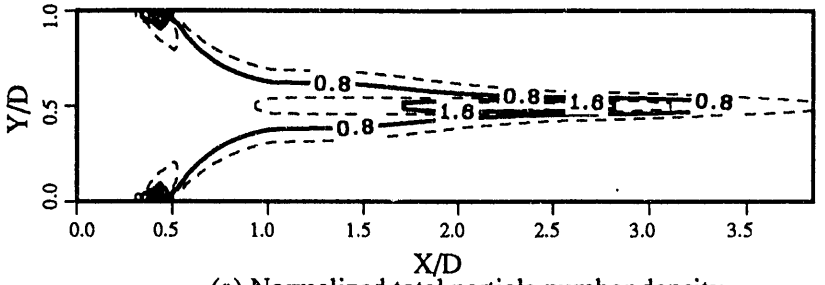

(a) Normalized total particle number density

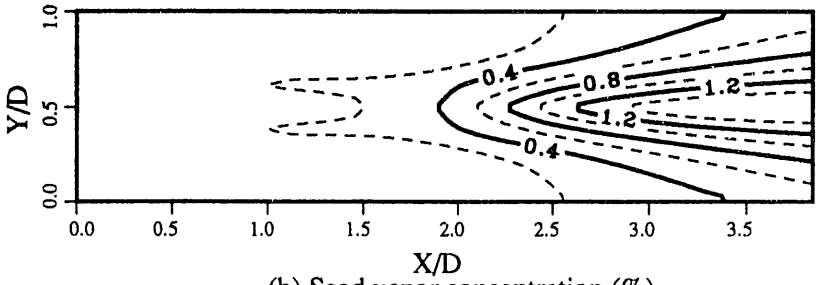

(b) Seed vapor concentration (%)

Figure 7 Seed particle evolution and vapor dispersion patterns

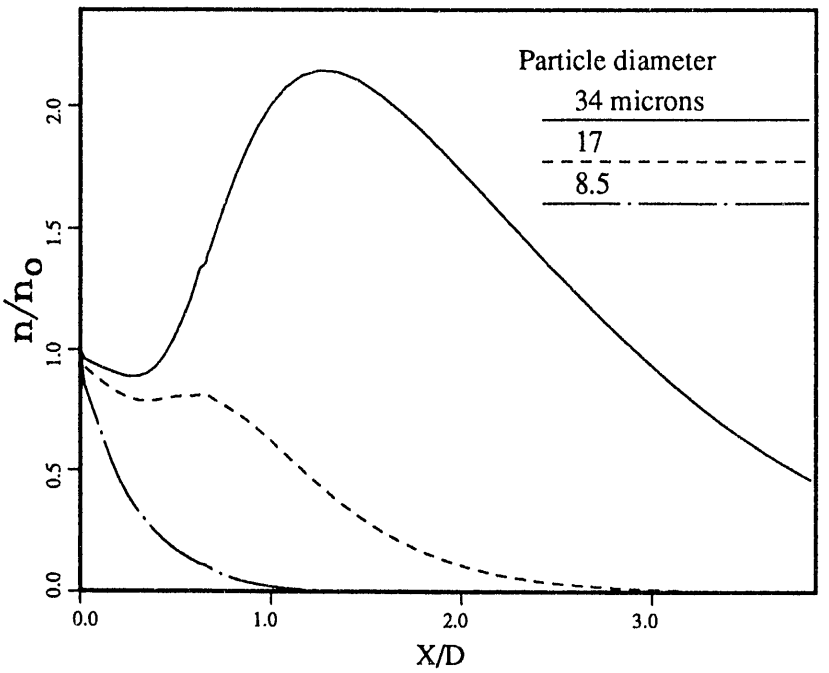

Figure 8 Centerline total number density of a particle laden combustion flow with various mean particle sizes

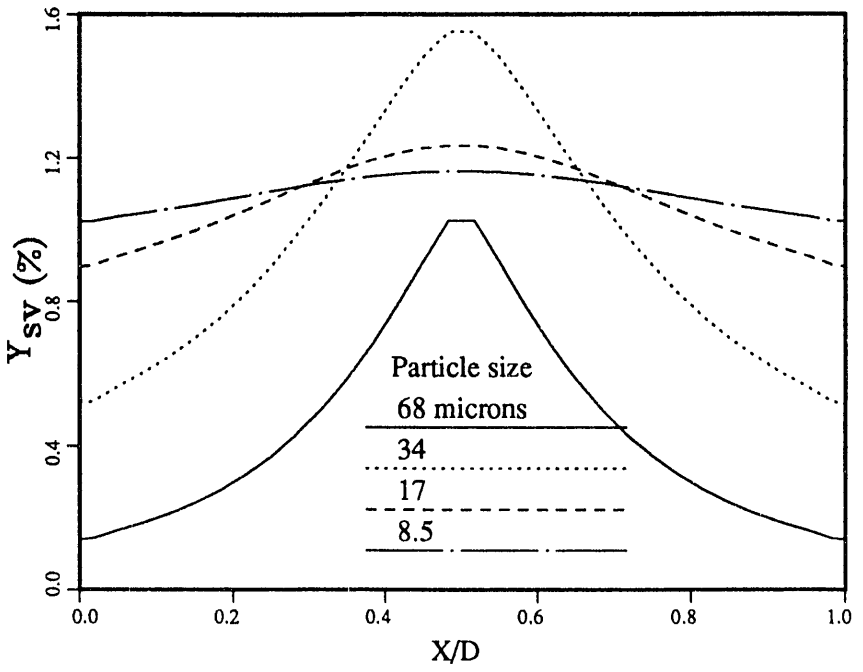

Figure 9 Comparison of exit seed vapor concentration profiles for various mean particle diameters

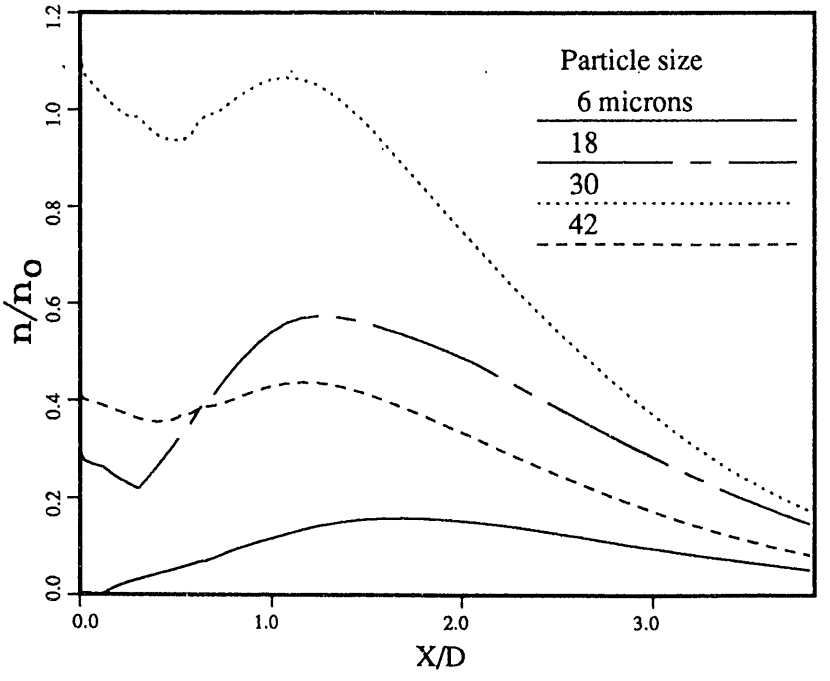

Figure 10 Centerline particle number density of individual size group

DATE
FILMED
2/9/93